59th ILMENAU SCIENTIFIC COLLOQUIUM
Technische Universität Ilmenau, 11 – 15 September 2017
URN: urn:nbn:de:gbv:ilm1-2017iwk-116:8

High precision electron-beam-lithography for optical high performance applications

Martin Heusinger[1]
Michael Banasch[2]
Uwe-Detlef Zeitner[1, 3]
Ernst-Bernhard Kley[1]

[1]Insitut für angewandte Physik, Friedrich-Schiller-Universität Jena
[2]Vistec Electron Beam GmbH, Jena
[3]Fraunhofer Institut für Optik und Feinmechanik, Jena

ABSTRACT

Due to its high resolution end flexibility, electron beam lithography (EBL) became an essential fabrication technique for micro-optical elements that are used in high performance applications. Nevertheless, the sequential writing strategy used in EBL enforces a stitching approach in order to fabricate large area micro-optical elements. Inherently, the stitching of special subareas leads to inaccuracies in the optical function of the fabricated micro-optics, which usually appears as stray light.

In this paper we report about a method to calibrate the stitching process and to reduce the stray light artefacts, respectively. The optimization method is based on the evaluation of angle resolved stray light measurements of special test gratings. In particular, the optimization concerns about spurious stray light peaks, also known as “Rowland ghosts”.

In a first step, the qualitative and quantitative characteristics of the observed Rowland ghosts are investigated in a theoretical model in order to deduce the modality of the stitching inaccuracy and the strength of the alignment error. In a second step, the calibration of the subarea-stitching is demonstrated on the example of a contemporary spectrometer grating. It is shown that the Rowland ghosts can be reduced significantly and the stitching process can be controlled in the nm-range.

1. INTRODUCTION

Electron beam lithography (EBL) is an established and versatile method, which allows fabricating micro-optical devices with a very high reliability and accuracy [1]. Due to the short de-Broglie wavelength of the accelerated electrons the resolution is not diffraction limited. Rather the electron optics and the scattering of the electrons in the resist and in the substrate are responsible for a limiting resolution, which therefor lies in the sub-10nm-range.

This benefit made EBL become an essential fabrication technology for optical high performance applications, e.g. like spectrometer gratings for astronomy and earth observation [2]. Such applications have special demands on various grating characteristics, e.g. diffraction efficiencies typically higher than 90%, a high spectral dispersion and a broad spectral bandwidth [3, 4]. In order to address these high demands on the optical function it is necessary to fabricate microstructures with an accuracy in the range of 10nm. EBL allows fabricating micro-optical elements that require such an accurate geometry of the diffractive structure.

Nevertheless, growing challenges of, e.g., contemporary spectrometers, which require large area gratings in the range of several 100 cm², push the e-beam writer to its limits. When

fabricating large area gratings a special writing strategy is necessary to address all regions of the grating by the electron beam within a feasible writing time. The so called *variable shaped beam* writing, which is depicted in Figure 1, can expose large areas within one shot and is thus significantly faster than *Gaussian beam* writing. The precise position of the electron beam is controlled by different deflection systems in the electron column and additionally the substrate to be exposed is mounted on a movable substrate stage. Hence, the grating is divided into several subareas that are sub-sequentially exposed and stitched together leading to the final full size grating. This division and assembly occur twice in our e-beam writer and the corresponding subareas are named SUB and Stripes (STR).

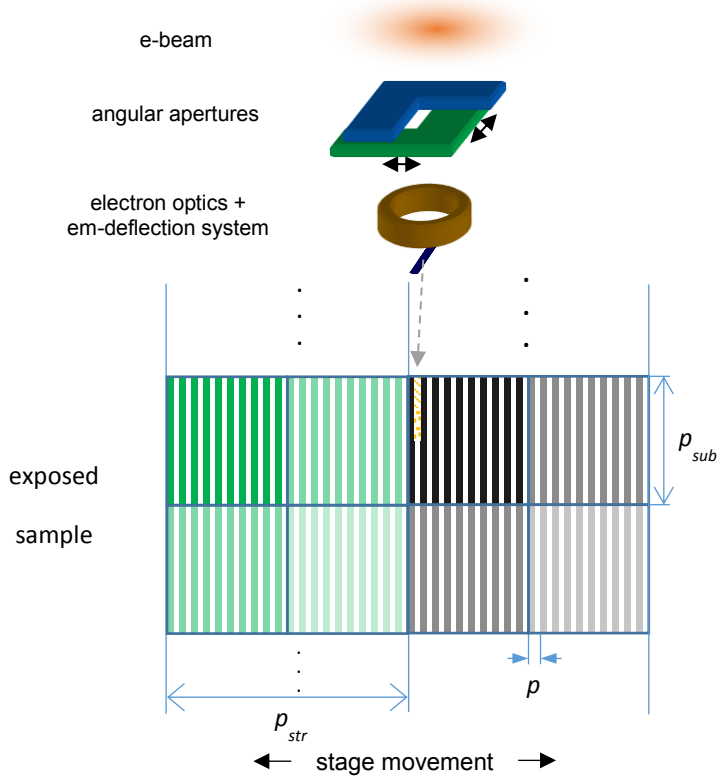

Figure 1: Illustration of the "variable shaped beam"-exposure principle in e-beam-lithography and origin of the structures that may cause the spurious stray light peaks.

Due to this stitching approach the subareas may induce secondary periodic structures that arise as super-periods p_{sub} and p_{str} next to the dominating grating period p. The established standard values in our e-beam-writer are $p_{sub} = 35\,\mu m$ and $p_{str} = 625\,\mu m$. In optical applications, these super-periods are prone to generate aberrations in the desired optical function. E.g., in spectrometer gratings the super-periods lead to periodic wavefront-errors and, thus, to the occurrence of spurious secondary diffraction orders, which we will refer to as stray light peaks and *Rowland ghosts*, respectively [5, 6]. Figure 2 shows an angle resolved stray light (ARS) measurement of a current spectrometer grating and reveals Rowland ghosts in the order of magnitude of $<10^{-4}$ compared to the useful diffraction order. According to the two different super-periods it is advisable to distinguish between the Rowland ghosts that arise from p_{sub} and p_{str}, respectively. In Figure 2 the Rowland ghosts that belong to the particular super-period are named as *SUB-ghosts* and *STR-ghosts*. Growing demands on the performance of spectrometer gratings and micro-optics in general require a reduction of the Rowland ghosts and an improvement of the subarea alignment, respectively. Hence, there is a need for a precise alignment control of the different subareas with respect to each other.

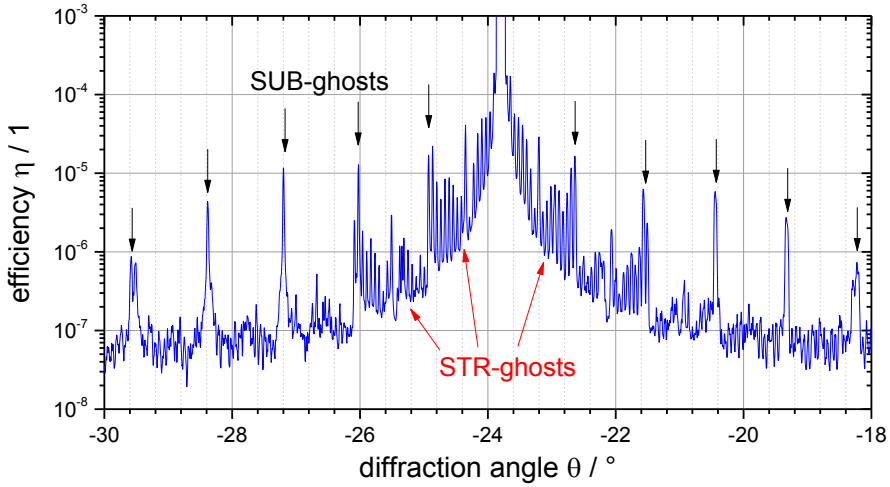

Figure 2: ARS measurement ±6° around the -1st diffraction order (at θ=-23.8°) of a current spectrometer grating. The Rowland ghosts are marked by black and red arrows according to the corresponding super-periods p_{sub} and p_{str}, respectively. Incidence angle $\theta_{inc} = 33°$, $p = 667\,nm$, $\lambda = 633\,nm$.

In this manuscript we will theoretically investigate the influence of alignment-errors on the stray light spectra of contemporary spectrometer gratings. We will show that the positioning-error of the SUBs and STRs in the nm-range can be evaluated by means of ARS measurements. Based on this, a precise alignment control of the subareas in the nm-range will be experimentally demonstrated. In particular, a reliable calibration of the SUB- and STR-nanopositioning by means of ARS measurements and a continuous reduction of the Rowland ghosts is performed.

2. MEASUREMENT SET-UP

The ARS in the dispersion direction of the grating was measured by the use of a double circle goniometer stage. The piezo controlled goniometer allows a positioning of the source and the detector with an accuracy of $\Delta\theta \approx 0.001°$. As the light source we used a Helium Neon laser with a wavelength of $\lambda = 632.8\,nm$ and a full width half maximum of less than $0.8\,nm$. Thus the measured ARS is free of dispersion artefacts of the incident laser beam. Further the light was coupled into a fiber that gives an almost perfect Gaussian beam profile and additionally allows a comfortable handling of the incident beam on the goniometer.

The beam was focused by a single lens through the sample onto a slit that is mounted in front of the detector. The slit has dimensions of $50\,\mu m \times 2.5\,mm$ and ensures that only signals in a small range around the adjusted scattering angle are measured. The light beam that is impinging onto the grating still has a diameter of about $15\,mm$. Thus a large number of subareas and single grating periods is illuminated and the resulting measurement is therefore representative for integrating effects like stray light. Furthermore this large illumination area allows a distinct propagation of the Rowland ghosts that arise from super periods in the range of $p_{str} = 625\,\mu m$.

As detector we used a conventional photodiode-detector that possesses a dynamic range of 4.5 orders of magnitude. With this set-up the measurement was restricted to an efficiency range of $10^{-4}\ldots10^{-8}$, stronger signals provoke a detector saturation and weaker signals are covered by thermal noise.

With a measured signal intensity $I_S(\theta_S)$ for an adjusted scattering angle θ_S and the reference signal of the incident beam I_0 the Rowland ghost intensity can be calculated by $\eta = I_S / I_0$.

3. SIMULATION OF THE EFFECT OF ALIGNMENT ERRORS ONTO THE STRAY LIGHT SPECTRA

3.1. Basic simulation principle

For the simulation of the light propagation through the grating and eventually of the intensity distribution in the full transmission half space a numerical algorithm based on the *rigorous coupled wave analysis* (RCWA) was applied. This method calculates the light propagation of an electromagnetic plane wave incident upon a periodically structured surface with period p [7]. The study presented in this work is based on a simple binary phase grating in fused silica with period p = 667 nm, duty cycle *f=0.65* and groove depth d = 1640 nm (the grating design is depicted in Figure 3). For an incidence angle $\theta_{inc} = 33°$ and a wavelength $\lambda = 632.8$ nm such a grating possesses only 2 propagating diffraction orders at $\theta_{-1} = -23.8°$ and $\theta_0 = 33°$. Scattered light in the angular range between the diffraction orders is caused by large scale variations of the ideal grating profile with typical length scales $P \gg p$. For simulating the intensity distribution of the scattered light we still use RCWA by introducing a super lattice with period $P = N \cdot p$. Such a compound of many single periods p possesses additional diffraction orders, e.g. there are 8 orders for N = 4 with the -4th order corresponding to the -1st order for N=1. The effect of increasing P is depicted in Figure 3. In order to simulate the intensity distribution of the Rowland ghosts that arise from subareas of the size $p_{sub} = 35\,\mu m$, the parameter has to be set $N_{sub} = 52$.

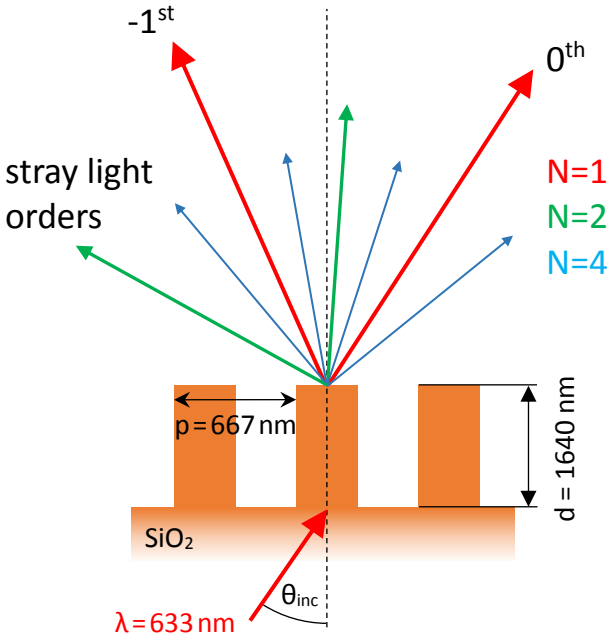

Figure 3: Geometry of the investigated grating and illustration of the stray light simulation principle. N represents the number of connected periods p in the RCWA algorithm. The red arrows are the main diffraction orders belonging to p. The green and blue arrows represent the additional stray light orders that arise if N>1.

Unfortunately, the described simulation principle is a very time-consuming numerical algorithm with a computation time proportional to N. Whereas the SUB-pattern can be simulated without exceeding numerical effort, it is not feasible to simulate the effects of the STR-pattern as $N_{str} = 937$. Therefore, the theoretical investigations will be restricted to only the SUB-pattern and it is assumed that the results are transferable to the STR-pattern.

3.2. Characteristic of the occurring alignment error

For simulating the scattering due to alignment-inaccuracies of the subareas it is convenient to distinguish between statistic and deterministic alignment-errors. Even if there is a perfect lateral alignment of the subareas, there is still an inevitable statistical positioning-error of the SUBs and STRs. Indeed, a statistic positioning error is very different to a deterministic error: The statistic error leads to a shift Δ_{stat} of the actual grating bar position from its ideal position. This shift is constant within one subarea for every grating bar, but individually different for every subarea. Δ_{stat} is a random number and assumed to be normally distributed described by a mean value $\langle\Delta_{stat}\rangle = 0$ and a standard deviation σ.

In contrast, the deterministic error can be described by a constant gap (or overlay) Δ_{det} between adjacent subareas, which results in a slightly increased (or reduced) subarea $p_{sub} = N_{sub}\, p + \Delta_{det}$. Even if Δ_{det} is small, the gap accumulates throughout the total grating area and leads to strong deviations of the actual bar position from the ideal bar position.

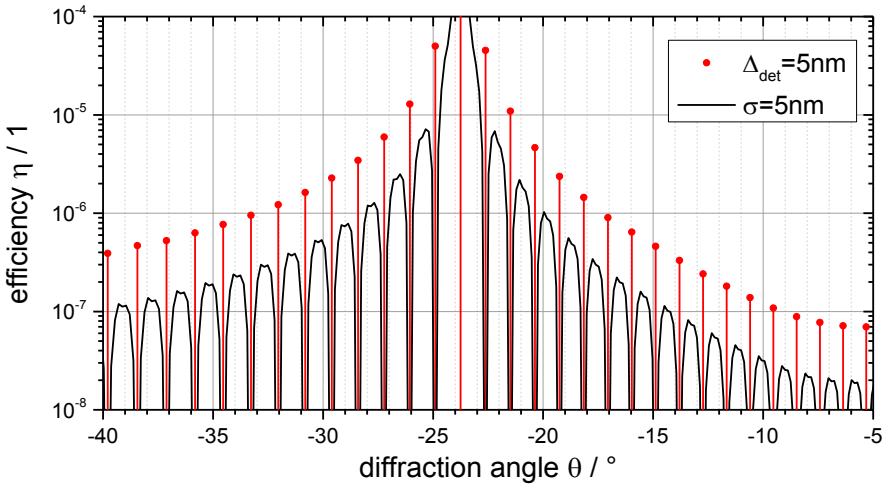

Figure 4: Simulated stray light spectra around the -1st diffraction order (at θ=-23.8°) originating in a deterministic and statistic alignment error, respectively. Incidence angle θ_{inc} = 33°, p = 667nm, λ = 633nm.

The simulation results for $\sigma = 5\,$nm and $\Delta_{det} = 5\,$nm are shown in Figure 4. The effects of both errors onto the stray light spectra are completely different. Whereas the deterministic alignment-error generates the expected Rowland ghosts, the statistic alignment-error generates a homogeneous scattering background with local minima at the positions of the expected Rowland ghosts. A comparison with the measurement presented in Figure 2, which shows Rowland ghosts occurring as distinct peaks in the spectrum, reveals that the main alignment error is based on deterministic positioning inaccuracies, whereas statistical errors are negligible. Further, we find a similar qualitative behavior of the measured and simulated Rowland ghosts. Close to the useful diffraction order at -23.8° the most intense Rowland ghosts can be found and their intensity continuously reduces with growing angular distance.

3.3. Strength of the alignment error and sensitivity of the ARS measurement

It has to be noted that there also might occur other effects, which potentially are able to generate Rowland ghosts, e.g. like an error in the uniformity of the exposure dose throughout a subarea [6]. Such effects are additive and would only increase the Rowland ghost intensity. Therefore, a comparison of simulated stray light data based on purely deterministic alignment errors with measurement data can only give an estimation of the maximum lateral alignment error that

occurs in the lithography process. E.g., Figure 5 shows several simulated scattering spectra with a variation of parameter Δ_{det} and a stray light measurement of a special test grating. It is found that a varying Δ_{det} only influences the strength of the Rowland ghosts but not their qualitative behavior. Further, a comparison of the simulated Rowland ghosts with a stray light measurement of a test grating reveals that there occurs typically a deterministic alignment error of less than 5 nm.

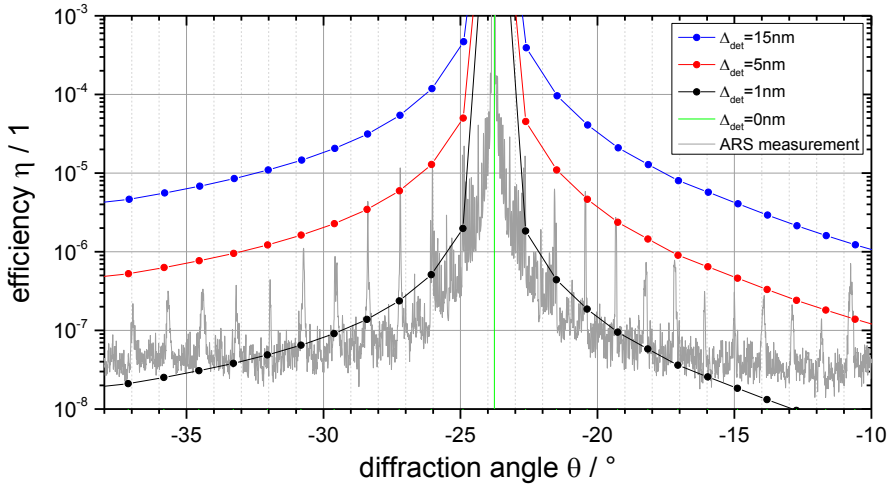

Figure 5: Comparison of the simulated Rowland ghosts for varying strength of the deterministic alignment error Δ_{det} with an ARS measurement around the -1st diffraction order (at θ=-23.8°) of a special test grating. Incidence angle θ_{inc} = 33°, p = 667 nm, λ = 633 nm.

The e-beam-machinery used for fabricating test gratings offers several calibration parameters that control the positioning of the subfields and stripes. Usually the stitching of the single subfields and stripes and in particular the calibration parameters are monitored regularly by the characterization of coordinate-positions of special test structures. This method is able to calibrate the local alignment state with a very high accuracy. Nevertheless, it can be deduced from Figure 5 that this method obviously is not applicable for integrating effects like stray light, where the global alignment accuracy has to be optimized. Therefore, the relevant calibration parameters must be determined by performing and evaluating stray light measurements. As can be seen in Figure 5, this method should have a sensitivity to determine a minimum alignment accuracy of $\Delta_{det,min} \approx 1$ nm.

4. CALIBRATION OF THE E-BEAM-WRITER BY MEANS OF STRAYLIGHT MEASURMENTS

In the used e-beam-writer *Vistec 350OS* the positioning of the SUB-pattern is controlled by the micro-deflection-system which can be tuned by parameter Δ_{sub}. On the other hand, the macro-deflection-system controls the STR-alignment and can be tuned by parameter Δ_{str}. In the following the influence of these parameters on the strength of the Rowland ghosts of several test gratings is investigated. Technically, the overlay (or gap) between adjacent subareas is a function of a set of machinery parameters. Therefore, the value of Δ_{sub} and Δ_{str} is given in arbitrary units. Nevertheless, the achieved alignment accuracy will be estimated in sec. 4.2.

In order to shorten the time consuming fabrication sequence of e-beam-exposure, resist (FEP171) development, chromium-mask-etching, deep SiO_2-etching and mask removal most ARS measurements are executed already after the resist development (resist thickness $d_{fep} = 300$ nm). The measurement was performed in reflection with an incidence angle of $\theta_{inc} = 20°$, which leads to a propagating -1st diffraction order at $\theta_{-1} = -37.4°$. Though, the finally

fabricated grating with optimized stray light performance is processed completely in order to show explicitly the applicability of the achieved improvements on deep gratings.

4.1. Macro-Deflection-System

In order to optimize the STR-stitching several gratings were fabricated with constant parameter Δ_{sub} and varying Δ_{str} and their ARS was measured. Figure 6 shows the best and the worst curve regarding the intensity of the STR-ghosts. We find that the strength of the STR-ghosts is considerably influenced by the calibration parameter Δ_{str}. In particular in the small angular range of ±1° around the -1^{st} DO almost all STR-ghosts decrease by actually one order of magnitude. On the other hand, it can be seen that the strength of the SUB-ghosts remains unaffected.

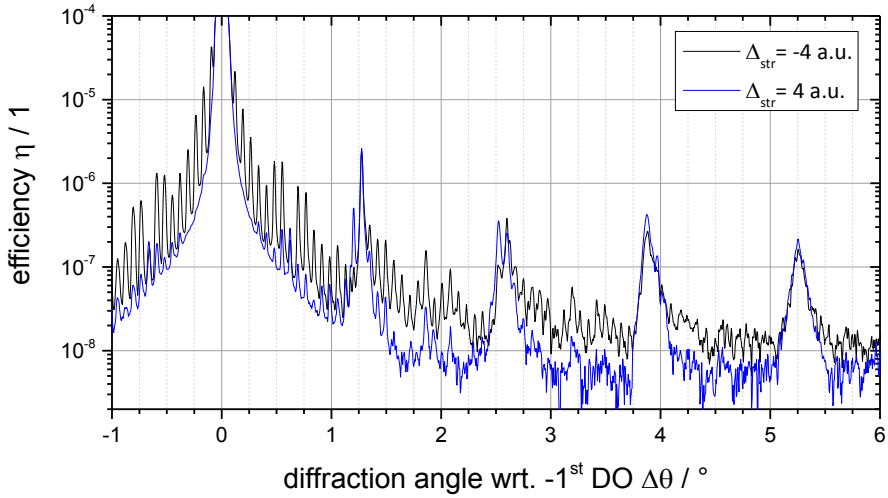

Figure 6: ARS measurement around the -1^{st} DO (at $\Delta\theta = 0°$) of two gratings fabricated with different STR-overlap. Incidence angle $\theta_{inc} = 20°$, $p = 667\,nm$, $\lambda = 633\,nm$.

4.2. Micro-Deflection System

Instead, the strength of the SUB-ghosts can be influenced by turning parameter Δ_{sub}. The ARS-measurements of two gratings fabricated with very different SUB-stitching is depicted in Figure 7. We find that the strength of the SUB-ghosts can be reduced significantly, e.g. the 1^{st} SUB-ghost next to the -1^{st} diffraction order (at $\Delta\theta = 1.3°$) decreases by almost 2 orders of magnitude. A simulation of the SUB-ghosts reveals that this corresponds to an alignment inaccuracy in the range of less than 1nm.

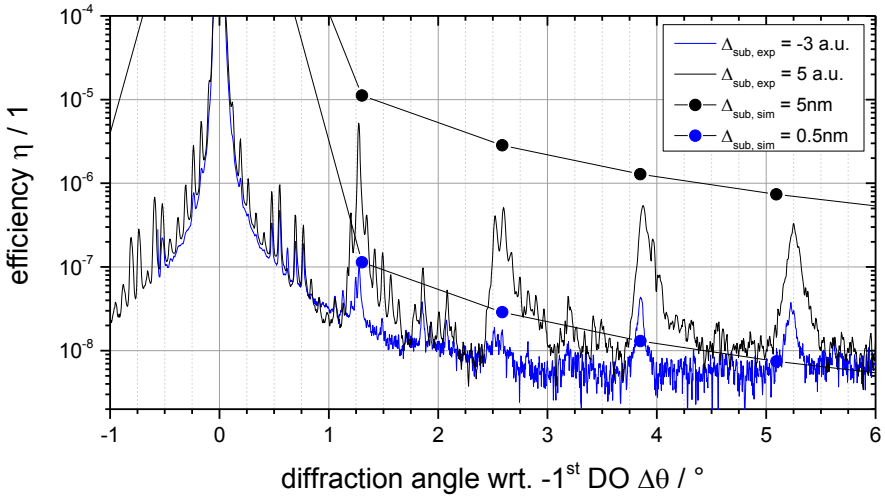

Figure 7: ARS measurement around the –1st DO (at $\Delta\theta = 0°$) of two gratings fabricated with different SUB-overlap. As an orientation the simulation results for different parameters Δ_{sub} are also shown. Incidence angle $\theta_{inc} = 20°$, $p = 667nm$, $\lambda = 633nm$.

4.3. Optimized SUB- and STR-alignment

Finally, the calibrated STR- and SUB-alignment via ARS measurements allows fabricating gratings with a minimum alignment error and optimized stray light performance. The remaining Rowland ghosts that appear in the measurement shown in Figure 7 can be further reduced by applying the well-known technique of the *"multi-pass-exposure"* [8]. Details about the effect of this method onto the scattering spectra can be found in [9].
However, an ARS measurement of a grating with optimized stitching process fabricated in the 8-pass exposure regime is shown in Figure 8. Here, the measurement was performed in transmission on a fully processed fused silica grating with an incident angle of $\theta_{inc} = 33°$. The measured angular range was $\Delta\theta = [-1°, \ldots, 10°]$ related to the -1^{st} diffraction order ($\theta_{-1} = -23.8°$). The comparison to the unoptimized grating emphasizes the improvement of the stray light performance. The alignment optimization allows a significant reduction of the Rowland ghosts by almost 2 orders of magnitude.

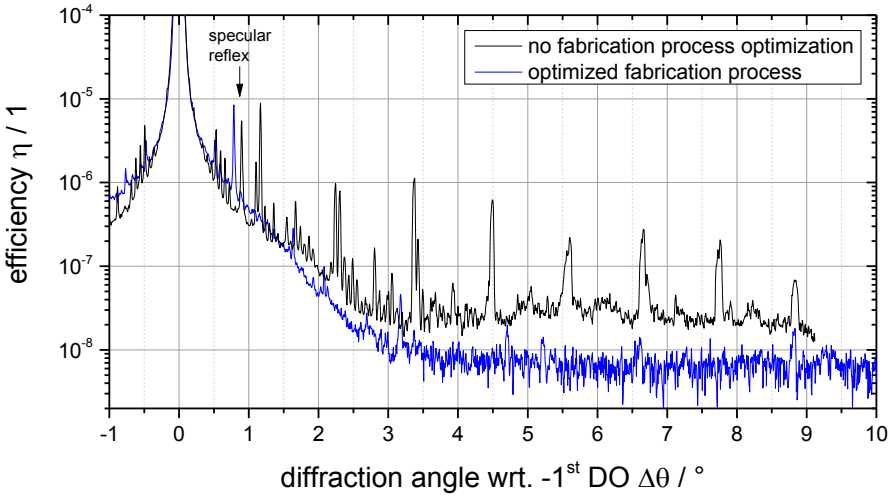

Figure 8: ARS measurement around the -1st diffraction order (at $\Delta\theta = 0°$) of an optimized and a not optimized diffraction grating. Incidence angle $\theta_{inc} = 33°$, $p = 667nm$, $\lambda = 633nm$.

5. CONCLUSION

In this manuscript we present a method that allows a precise calibration of the stitching of special subareas that occur in electron beam lithography in order to fabricate large area micro-optical elements. The method is based on the evaluation of angle resolved stray light measurements of special test gratings. In particular, the qualitative and quantitative appearance of deterministic stray light peaks, so called Rowland ghosts, are related to the modality and the strength of the alignment error. It is shown that the origin of the Rowland ghosts must be purely systematic and, thus, that the Rowland ghosts can be used in order to optimize the stitching process and the alignment accuracy, respectively.

Based on this findings, an optimization is exemplarily demonstrated on a current high performance spectrometer grating. The Rowland ghosts in such a grating typically have a strength of less than 10^{-4} compared to the useful diffraction order. As a result, the calibration state of the e-beam-writer was found to have a deterministic alignment error of 5 nm, which was reduced to a minimum error in the range of 1 nm. This corresponds to a reduction of the Rowland ghosts of almost 2 orders of magnitude.

REFERENCES

[1] U. D. Zeitner, M. Oliva, F. Fuchs, D. Michaelis, T. Benkenstein, T. Harzendorf, and E.-B. Kley, *"High performance diffraction gratings made by e-beam lithography,"* Appl. Physics A **109**(4), 789-796, 2012.

[2] U. D. Zeitner, F. Fuchs, and E.-B. Kley, *"High-performance dielectric diffraction gratings for space applications,"* Proc. SPIE **8450**, 84502Z, 2012.

[3] S. Kraft, U. Del Bello, B. Harnisch, M. Bouvet, M. Drusch, and J.L. Bézy, *"Fluorescence Imaging Spectrometer concepts for the Earth Explorer Mission Candidate FLEX,"* Proc. SPIE **8889**, 88890T, 2013.

[4] D.R. Lobb and I.S. Bhatti, *"Applications of immersed diffraction gratings in earth observation from space,"* Proceedings of the ICSO—International Conference on Space Optics, 2010.

[5] C. A. Palmer, E. G. Loewen, and R.G.L. Thermo, *Diffraction grating Handbook*, Newport Corporation, Springfield, 2005.

[6] M. Heusinger, T. Flügel-Paul, and U.D. Zeitner, *"Large-scale sementation errors in optical gratings and their unique effect onto optical scattering spectra,"* Appl. Physics B **122**(8), 222, 2016.

[7] M.G. Moharam, T.K. Gaylord, E.B. Grann, and D.A. Pommet, *"Formulation for stable and efficient implementation of the rigorous coupled-wave analysis of binary gratings,"* JOSA A **12**(5), 1068–1076, 1995.

[8] C. N. Berglund, J. R. Thomas, and J. T. Poreda, *"Multiphase printing for E-beam lithography,"* U.S. patent No. 5, 103, 101, 1992.

[9] M. Heusinger, M. Banasch, and U.D. Zeitner, *"Rowland ghosts suppression in high efficiency spectrometer gratings fabricated by e-beam-lithography,"* Optics Express **25**(6), 6182-6191, 2017.

CONTACTS

Dipl.-Phys. M. Heusinger martin.heusinger@uni-jena.de